I. S. Nikitin, N. G. Burago, A. D. Nikitin, B. A. Stratula, Multi-mode Model and Calculation Method for Fatigue Damage Development. In book: Applied Mathematics and Computational Mechanics for Smart Applications. Proceedings of AMMAI 2020 Serie: Smart Innovation, Systems and Technologies. Vol: 217. Chapter 12, 2021. Springer Nature Singapore Pte Ltd Singapore pp. 157-170. DOI: 10.1007/978-981-33-4826-4_12

## Chapter 12

# Multi-Mode Model and Calculation Method for Fatigue Damage Development

Ilia S. Nikitin[1,a,*[0000-0003-3499-6910]], Nikolay G. Burago[1,b[0000-0002-1806-9386]], Alexander D. Nikitin[1,c[0000-0002-2916-758X]] and Boris A. Stratula[1,d[0000-0001-8916-5263]]

[1] Institute for Computer Aided Design of the RAS (ICAD RAS), 19/18, Vtoraya Brestskaya ul., Moscow, 123056 Russian Federation
i_nikitin@list.ru[a], buragong@yandex.ru[b], nikitin_alex@bk.ru[c], stratula@matway.net[d]

**Abstract.** A multi-mode kinetic model of damage development under cyclic loading is proposed to describe the process of fatigue failure. To determine the coefficients of the kinetic equation of damage, the well-known criterion of multiaxial fatigue failure is used. A procedure is proposed for calculating the kinetic equation coefficients for various fatigue failure modes of the LCF-HCF and VHCF. A numerical method for calculating crack-like zones up to macrofracture is developed. The model parameters are determined from the condition of matching the experimental and calculated fatigue curve for a specimen of a certain geometry at a given load amplitude and cycle asymmetry coefficient. Using the obtained values, the results of experiments on specimens of a different geometry and asymmetry coefficients were reproduced and the model and calculation algorithm performance was confirmed.

**Keywords:** Fatigue, Damage Development, Multi-mode Model, High Cycle Fatigue, Very High Cycle Fatigue

## 12.1 Introduction

Entire classes of criteria have been constructed that relate the number of cycles before the initiation of fatigue damage (microcracks) with the amplitudes and maximum values in the cycle (or average) that characterize the uniform stress-strain state of the working part of the specimen in a fatigue test.

A large number of stress-based criteria are based on a direct generalization of the S-N Wöhler-type curves described by Basquin-type relations [1], and based upon the results of fatigue tests. The main criteria for multiaxial fatigue failure, taking into account the values of strain amplitudes (strain-based criteria), were proposed in [2-4]. These criteria are divided into two large groups. The first group includes criteria that use the amplitudes of the invariant characteristics of the stress state in the loading cycle such as octahedral stresses, principal stresses, etc. [5,6], and the second group

includes criteria that take into account the amplitudes of the tangent and/or normal stresses on the so-called critical plane [7-14]. As a rule, this plane is determined from the condition of the maximum amplitudes of the tangent, normal stresses, or a certain combination of them on the planes of various orientations. Reviews on this topic are given, say, in [15-19].

In order to study the development of fatigue damage zones, there are also two approaches. The first is based on the classical concepts of fracture mechanics and relates the conditions for the development of fatigue cracks depending on the amplitudes of stress intensity factors at the crack tip with the increase in the number of cycles. The basic equation was proposed by Paris and Erdogan [20], there are a large number of modifications of it [21-23]. The second approach uses representations of the theory of damage, dating back to [24–25] and developed in [26–28]. As applied to the problems of cyclic loading and fatigue failure, it was used in [29–32].

We study the processes of fatigue damage zones development using the damage theory approach dating back to [24, 25]. In the application to the cyclic loading and fatigue failure problems, this approach was applied in [27, 28]. We propose a multimode model for the development of fatigue failure based on the evolutionary equation for the damage function. The model parameters are determined for various modes of fatigue failure: Low-Cycle Fatigue (LCF) and High-Cycle Fatigue (HCF), as well as, the regime of Very-High-Cycle Fatigue (VHCF), corresponding to high-frequency low-amplitude loading.

To distinguish the various modes of fatigue failure, we use the multimode amplitude fatigue curve diagram shown in Fig. 12.1. Up to a value of $N \sim 10^3$, the regime of re-static loading is realized with an amplitude that differs little from the static strength limit $\sigma_B$. Further, the left part of the bimodal fatigue curve (Wöhler curve) describes LCF-HCF modes up to $N \sim 10^7$ and amplitude values of the order of the fatigue limit $\sigma_u$. Then begins the zone of change of fracture mechanisms and a further drop in fatigue strength, starting from $N \sim 10^8$ to a new fatigue limit value $\tilde{\sigma}_u$ in accordance with the right branch of the bimodal S-N fatigue curve. This branch describes VHCF mode [33].

It should be noted that at present, the idea of an explicit division of the classic Wöhler branch into two parts (in fact, LCF and HCF) exists. The boundary of this transition region is determined not by the value of *N*, but by the value of the loading amplitude equal to the yield strength of the material $\sigma_T$ [34], since this changes the physical mechanism of fatigue failure. In addition, the boundary of the repeated-static range $N \sim 10^3$ is rather arbitrary. It is also specified in [34] depending on the strength and plastic characteristics of the material. However, in this chapter we keep the suggestion of the proposed model of damage development based on the scheme described above.

In order to match the model with the well-known criteria for multiaxial fatigue failure, a stress-based criterion has been selected that describes the fatigue failure associated with the normal crack microcracks development. This is a modification of the Smith-Watson-Topper (SWT) criterion [4] described in [35], in which the ampli-

tudes of maximum tensile stresses play a decisive role in the development of fatigue damage.

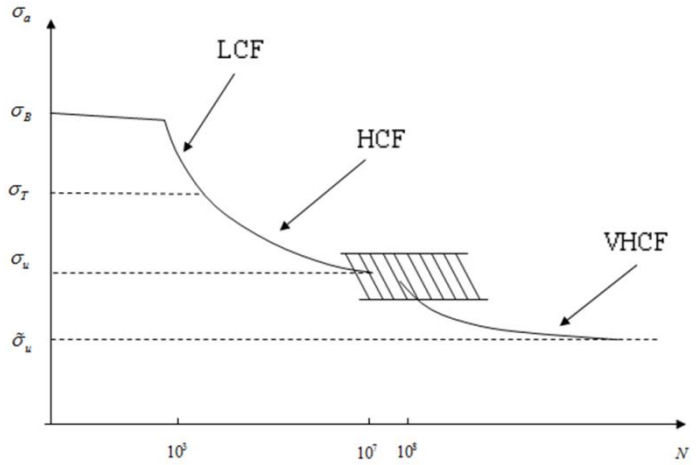


**Fig. 12.1.** Bimodal fatigue curve.

This chapter is organized as follows: Section 12.2 presents kinetic equations for two fatigue modes and a condition to switch between them. Algorithm for fatigue damage development calculation is presented in Sect. 12.3. Section 12.4 is dedicated to calculation results both in LCF-HCF and VHCF modes. Section 12.5 concludes the chapter.

## 12.2 Kinetic Equation for Damage

In this work, two different modes of fatigue loading are studied: classic LCF-HCF mode and VHCF mode in Sects. 12.2.1 and 12.2.2, respectively. Also an algorithm to choose between them is presented in Sect. 12.2.3.

### 12.2.1 LCF-HCF Mode

The criterion of multiaxial fatigue failure in LCF-HCF mode with the development of normal crack microcracks [35] (stress-based SWT) corresponding to the left branch of the bimodal fatigue curve (Fig. 12.1) is

$$\sqrt{\left\langle \sigma_{1_{\max}} \right\rangle \Delta\sigma_1 / 2} = \sigma_u + \sigma_L N^{-\beta_{LH}} , \tag{12.1}$$

where $\sigma_1$ is the largest principal stress, $\Delta\sigma_1$ is the range of the largest principal stress per cycle, $\Delta\sigma_1 / 2$ is the amplitude. From the condition of repeated-static fracture up to values of $N \sim 10^3$ by the method [19] it is possible to obtain the value

$\sigma_L = 10^{3\beta_{LH}}(\sigma_B - \sigma_u)$. According to the chosen criterion only tensile stresses lead to failure, thus it includes the value $\left\langle \sigma_{1_{\max}} \right\rangle = \sigma_{1_{\max}} H(\sigma_{1_{\max}})$. In these formulas $\sigma_B$ is the static tensile strength of the material, $\sigma_u$ is the classic fatigue limit of the material during a reverse cycle (asymmetry coefficient of the cycle $R$ = -1), $\beta_{LH}$ is power index of the left branch of the bimodal fatigue curve.

From the fatigue fracture criterion we obtain the number of cycles before fracture at uniform stressed state:

$$N_{LH} = 10^3 \left[ (\sigma_B - \sigma_u) / \left\langle \sigma_{LH} - \sigma_u \right\rangle \right]^{1/\beta_{LH}}, \quad \sigma_{LH} = \sqrt{\left\langle \sigma_{1_{\max}} \right\rangle \Delta\sigma_1 / 2}. \qquad (12.2)$$

In order to describe the process of fatigue damage development in LCF-HCF mode, a damage function $0 \le \psi(N) \le 1$ is introduced, which describes the process of gradual cyclic material failure. When $\psi = 1$, a material particle is considered completely destroyed. Its Lame modules become equal to zero. The damage function $\psi$ as a function on the number of loading cycles for LCF-HCF mode is described by the kinetic equation:

$$d\psi / dN = B_{LH} \psi^{\gamma} / (1 - \psi^{\alpha}),$$

where $\alpha$ and $0 < \psi < 1$ are the model parameters that determine the rate of fatigue damage development. The choice of the denominator in this two-parameter equation, which sets the infinitely large growth rate of the zone of complete failure at $\psi \to 1$, is determined by the known experimental data on the kinetic growth curves of fatigue cracks, which have a vertical asymptote and reflects the fact of their explosive, uncontrolled growth at the last stage of macro fracture.

An equation for damage of a similar type was previously considered in [29], its numerous parameters and coefficients were determined indirectly from the results of uniaxial fatigue tests. In our case, the coefficient $B_{LH}$ is determined by the procedure that is clearly associated with the selected criterion for multiaxial fatigue failure of one type or another. It has the following form. The number of cycles to complete failure $N_{LH}$ at $\psi = 1$ is defined from the equation for damage for a uniform stress state provided by Eqs. 12.3.

$$\begin{aligned} &\left[ \psi^{1-\gamma} / (1-\gamma) - \psi^{(1+\alpha-\gamma)} / (1+\alpha-\gamma) \right]\Big|_0^1 = B_{LH} \, N\Big|_0^{N_{LH}} \\ &N_{LH} = \alpha / (1+\alpha-\gamma) / (1-\gamma) / B_{LH} \end{aligned} \qquad (12.3)$$

By equating the values $N_{LH}$ from the fracture criterion (Eq. 12.2) and from the solution of the equation for damage (Eqs. 12.3), we obtain the expression for the coefficient $B_{LH}$:

$$B_{LH} = 10^{-3}\left[\left\langle \sigma_{LH} - \sigma_u \right\rangle / (\sigma_B - \sigma_u)\right]^{1/\beta_{LH}} \alpha / (1+\alpha-\gamma) / (1-\gamma),$$

where the value $\sigma_{LH}$ is determined by the selected mechanism of fatigue failure and the corresponding multiaxial criterion (Eq. 12.1).

### 12.2.2 VHCF Mode

The criterion of multiaxial fatigue failure in VHCF mode corresponding to the right branch of the bimodal fatigue curve (generalized stress-based SWT) (Fig. 12.1) has the form:

$$\sqrt{\left\langle \sigma_{1_{\max}} \right\rangle \Delta\sigma_1 / 2} = \tilde{\sigma}_u + \sigma_V N^{-\beta_{VH}} .$$

Here, from the similarity condition of the control points for the left and right branches of the bimodal fatigue curve [33], we can obtain the formula:

$$\sigma_V = 10^{8\beta_{VH}} (\sigma_u - \tilde{\sigma}_u).$$

From the criterion of fatigue failure, we obtain the number of cycles to failure in a uniform stress state:

$$N_{VH} = 10^8 \left[(\sigma_u - \tilde{\sigma}_u) / \left\langle \sigma_{VH} - \tilde{\sigma}_u \right\rangle\right]^{1/\beta_{VH}}, \quad \sigma_{VH} = \sigma_{LH} = \sqrt{\left\langle \sigma_{1_{\max}} \right\rangle \Delta\sigma_1 / 2},$$

where $\tilde{\sigma}_u$ is the fatigue limit of the material during the reverse cycle for VHCF mode, $\beta_{VH}$ is the power-law index of the right branch of the bimodal fatigue curve.

### 12.2.3 Condition for Switching the Modes of Accumulation of Fatigue Damage

The transition point from the left branch of the fatigue curve to the right branch, at which the mechanism of fatigue fracture changes, is slightly above the fatigue limit $\sigma_u$ (Fig. 12.1) and is determined by the value $\sigma_* = \sigma_u + \Delta\sigma$. To ensure continuous conjugation of the left and right branches of the fatigue curve, it is necessary to fulfill a condition $N_{LH} = N_{VH}$ that is equivalent to the equation for the quantity $\Delta\sigma$:

$$10^3 \left[(\sigma_B - \sigma_u) / \left\langle \Delta\sigma \right\rangle\right]^{1/\beta_{LH}} = 10^8 \left[(\sigma_u - \tilde{\sigma}_u) / \left\langle \sigma_u + \Delta\sigma - \tilde{\sigma}_u \right\rangle\right]^{1/\beta_{VH}}$$

or

$$\Delta\sigma = 10^{-5\beta_{LH}} (\sigma_B - \sigma_u)\left[1 + \Delta\sigma / (\sigma_u - \tilde{\sigma}_u)\right]^{\beta_{LH}/\beta_{VH}}.$$

Given the actual smallness of the correction term in square brackets, one can set the correction value $\Delta\sigma$ by an approximate formula:

$$\Delta\sigma = 10^{-5\beta_{LH}}(\sigma_B - \sigma_u).$$

The corresponding approximate value $N_* = N_{LH}(\sigma_*)$ is determined by

$$N_* = 10^3\left[(\sigma_B - \sigma_u)/\Delta\sigma\right]^{1/\beta_{LH}} \approx 10^8.$$

Given the updated estimates obtained for the transition point from one branch of the fatigue curve to another, we obtain the final formulas for the ranges and coefficients of the kinetic equations of damage.

For LCF-HCF mode when $\sigma_u + \Delta\sigma_u < \sigma_{LH} < \sigma_B$ and $\Delta\sigma = 10^{-5\beta_{LH}}(\sigma_B - \sigma_u)$, we obtain:

$$B_{LH} = 10^{-3}\left[\left\langle\sigma_{LH} - \sigma_u\right\rangle/\left(\sigma_B - \sigma_u\right)\right]^{1/\beta_{LH}} \alpha/\left(1+\alpha-\gamma\right)/\left(1-\gamma\right),$$

$$\sigma_{LH} = \sqrt{\left\langle\sigma_{1_{\max}}\right\rangle\Delta\sigma_1/2}.$$

For VHCF mode when $\tilde{\sigma}_u < \sigma_{VH} \le \sigma_u + \Delta\sigma_u$, we have:

$$B_{VH} = 10^{-8}\left[\left\langle\sigma_{VH} - \tilde{\sigma}_u\right\rangle/\left(\sigma_u - \tilde{\sigma}_u\right)\right]^{1/\beta_{VH}} \alpha/\left(1+\alpha-\gamma\right)/\left(1-\gamma\right),$$

$$\sigma_{VH} = \sqrt{\left\langle\sigma_{1_{\max}}\right\rangle\Delta\sigma_1/2}.$$

When $\sigma_{VH} \le \tilde{\sigma}_u$, fatigue failure doesn't occur; when $\sigma_{LH} \ge \sigma_B$, it happens instantly.

## 12.3 Fatigue Damage Development Calculation Algorithm

Section 12.3 presents the approach to implement fatigue damage and calculate one's development. Ansys software was used to calculate the stress state within a loading cycle of a deformable specimen supplemented by a code to calculate the damage equation and changes of elasticity modulus.

To integrate the equation $d\psi/dN = B\psi^{\gamma}/(1-\psi^{\alpha})$, where $B$ either $B_{LH}$ or $B_{VH}$, the damage function approximation was applied at the *k*-node of the computational grid for given discrete values $\psi_k^n$ at moments $N^n$ and sought $\psi_k^{n+1}$ at moments $N^{n+1}$. To calculate the damage equation, the value $\alpha = 1-\gamma$ was chosen for which by analytic integration an explicit expression for $\psi_k^{n+1}(\psi_k^n, \Delta N^n)$ can be obtained:

$$\left[\psi^{1-\gamma}/(1-\gamma) - \psi^{2(1-\gamma)}/2/(1-\gamma)\right]\Big|_{\psi_k^n}^{\psi_k^{n+1}} = B\,N\Big|_{N_n}^{N_{n+1}}.$$

With the denotations $(\psi_k^{n+1})^{1-\gamma} = x$, $q = 2(1-\gamma)B\Delta N^n + (\psi_k^n)^{1-\gamma} - 2(\psi_k^n)^{2(1-\gamma)}$ and $\Delta N^n = N^{n+1} - N^n$ the equation transforms to $x^2 - 2x + q = 0$ and its valid root $x = 1 - \sqrt{1-q} < 1$. The analytical expression for the increment of damage on the increment of the number of cycles $\Delta N^n$ is derived from:

$$\psi_k^{n+1} = \left(1 - \sqrt{1 - \left[2(1-\gamma)B\Delta N^n + (\psi_k^n)^{1-\gamma} - 2(\psi_k^n)^{2(1-\gamma)}\right]}\right)^{1/(1-\gamma)}.$$

Increment value $\Delta N^n$ defined as follows. Based on the stress state calculation data, the coefficient $B = B_{LH}, B_{VH}$ is calculated for each node. After that, for each node, the following values are calculated by

$$\Delta\tilde{N}_k^n = \left[\psi^{1-\gamma}/(1-\gamma) - \psi^{2(1-\gamma)}/2/(1-\gamma)\right]\Big|_{\psi_k^n}^{1} / B$$

corresponding to the number of cycles, at which in the node *k* from its current level of damage and equivalent stress complete destruction will be achieved (damage is equal to 1). If the damage level in the considered node is less than the threshold $\psi_0$ (threshold $\psi_0 = 0.95$ is selected), then the value for this node $\Delta\tilde{N}_k^n$ is multiplied by a factor of 0.5. Otherwise, it is multiplied by a factor of 1. Thus, the step of incrementing the number of cycles for a given node is $\Delta N_k^n = 0.5(1 + H(\psi_k^n - 0.95))\Delta\tilde{N}_k^n$. Of all the $\Delta N_k^n$ values, the smallest one is selected. The increment of the number of loading cycles for the calculation of the entire specimen is $\Delta N^n = \min_k \Delta N_k^n$. For each node based on its current level of damage and equivalent voltage, a new level of damage is found taking into account the calculated increment $\Delta N^n$.

All elements are sorted out, for each of them the most damaged node is searched and according to its damage the mechanical properties of the element are adjusted:

$$\lambda(\psi_k^n) = \lambda_0(1 - \kappa\psi_k^n), \quad \mu(\psi_k^n) = \mu_0(1 - \kappa\psi_k^n).$$

Those elements that belong to nodes with damage $\psi = 1$ are removed from the calculation area and form a localized zone (crack-like) of completely destroyed material. The calculation ends when the boundaries of a completely damaged region exit to the specimen surface (macro destruction) or the evolution of this region stops.

## 12.4 Calculation results

Calculation of S-N curves and fatigue cracks propagation performed both in LCF-HCF and VHCF modes are presented in Sect. 12.4.

To determine parameters of the proposed model and verify its performance, one of the fatigue experiments described in [29] was performed numerically. From the con-

dition of matching the experimental and calculated fatigue curve for a specimen of certain geometry for a given loading amplitude and cycle asymmetry the numerical coefficients were found. Using the obtained values, the experimental results on specimens of a different geometry and asymmetry coefficients were reproduced, and calculation algorithm operability was confirmed.

Hereinafter, the numerical results for LCH-HCF mode and VHCF mode are discussed in Sects. 12.4.1 and 12.4.2, respectively.

### 12.4.1 Results for LCH-HCF Mode

Initial tests were conducted on a plate 100×25×1.57 mm in size with 1.56 mm diameter through hole in the ones center. Ratification tests were conducted on a V-notched specimen that has 15 mm width w/o a notch, thickness of 1.7 mm, the notch depth of 1.32 mm, the V-notch angle of 60 degrees, and the notch radius of 0.675 mm. The cyclic loading of the upper and lower boundaries of the specimen with amplitude of 0.096 mm with the development of damage zones up to macroscopic destruction was simulated and matched with the results from [29]. In the center of the plate, there is a through hole with diameter of 1.56 mm. Plate material is titanium alloy with strength and fatigue parameters $\sigma_B$ = 1135 MPa, $\sigma_u$ = 330 MPa, $\beta_{LH}$ = 0.31. Elasticity modulus of intact alloy are $\lambda_0$ = 77 GPa, $\mu_0$ = 44 GPa. Figs. 12.2 and 12.4 show the lines of the effective stress level $\sigma_{LH}$ for the specimen with a hole (Fig. 12.2) and for the specimen with a notch (Fig. 12.4) in two states: before the fatigue quasi-crack initiation and at the moment when it has passed approximately halfway to macro-destruction.

In Figs. 12.3 and 12.5, the results of real and computational experiments on constructing fatigue curves for specimens with a hole and a side notch are presented. Both real and calculated points represent the moment of a crack initiation. The curves in the figures approximate the experimental points. The calculations presented in Fig. 12.3b almost exactly fit the approximation curve for the values of the model parameters $\gamma = 0.1$ and $k = 0.5$. Utilizing these parameters, the fatigue curves presented in Fig. 12.3a (specimen with a hole, $R = -1$) and in Fig. 12.5 (notched specimen, $R = -0.5$ and $R = 0.1$). In Fig. 12.3b, the relative error equals 0 for the calibration series. The average relative errors in Figs. 12.3a, 12.5a and 12.5b are 1%, 7%, and 6%, respectively. The obtained satisfactory quality reproduction of real fatigue experiments indicates the efficiency and prospects of the model and calculation algorithm. The considered model represents the development of the damage model in case of cyclic loads presented in [36] for the description of damages during dynamic loading.

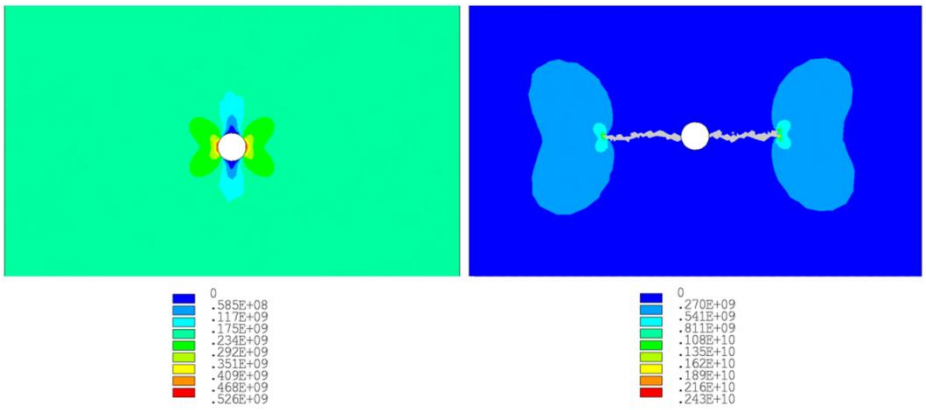


a b

**Fig. 12.2.** Ti-alloy specimen with a hole at $R = -1$: **a** emergence of a "quasi-crack", **b** growth of a "quasi-crack".

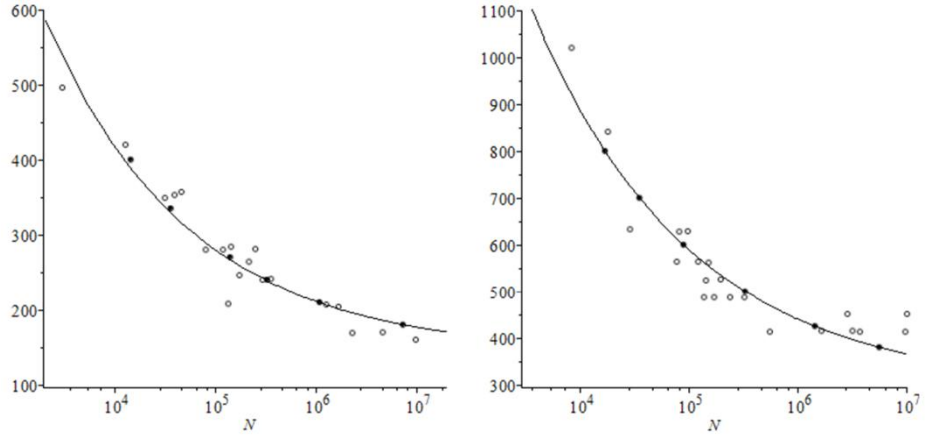


a b

**Fig. 12.3.** Fatigue curves $\sigma_{\max}(N)$ for Ti-alloy specimen with a hole, where ○ means real test points, ● means calculating points: **a** $R = -1$, **b** $R = 0.54$.

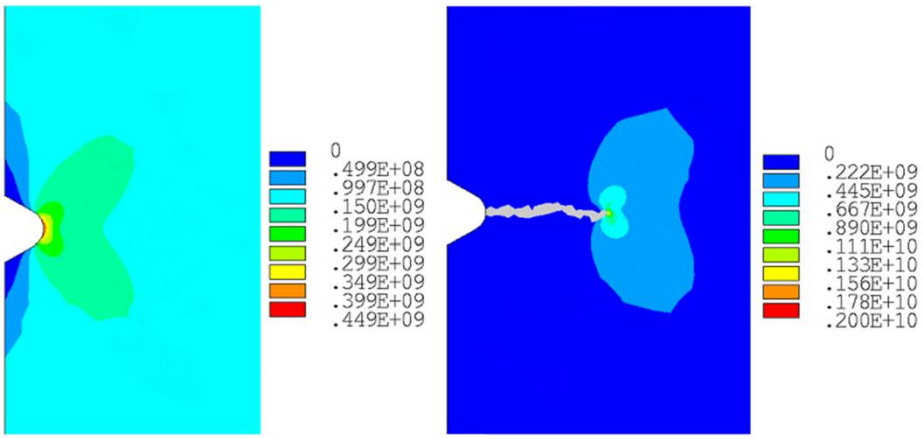


**Fig. 12.4.** V-notched Ti-alloy specimen at $R = -0.5$: **a** emergence of a "quasi-crack", **b** growth of a "quasi-crack".

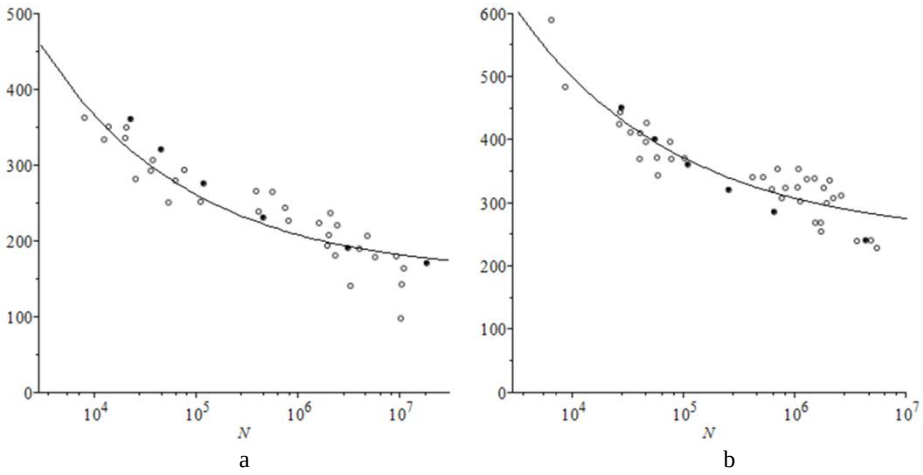


**Fig. 12.5.** Fatigue curves $\sigma_{\max}(N)$ for V-notched Ti-alloy specimen, where ◦ means real test points, ● means calculating points: **a** $R = -0.5$, **b** $R = 0.1$.

### 12.4.2 Results for VHCF Mode

In order to numerically investigate the development of crack-like regions of fatigue failure in UHMW mode, the cyclic loading of a specimen made of AS7G06-T6 aluminum alloy with reduced displacement amplitude of 0.1 mm was calculated. The corresponding experimental results are taken from the [37]. The mechanical properties of the Al-alloy: density $\rho$ = 2680 kg/m3, $E$ = 68 GPa, tensile strength $\sigma_B$ = 288

MPa, HCF fatigue limit $\sigma_u$ = 130 MPa, VHCF fatigue limit $\tilde{\sigma}_u$ = 60 MPa, $\beta_{VH}$ = 0.3.

In the series of tests, the bi-curved notched specimen shape was used. In the waist, it has quasi-flat shape of 6.18 mm width and 3 mm thick. The notch was 1 mm depth with the tip curvature radius of 0.5 mm and the angle of cleavage of 60 degrees.

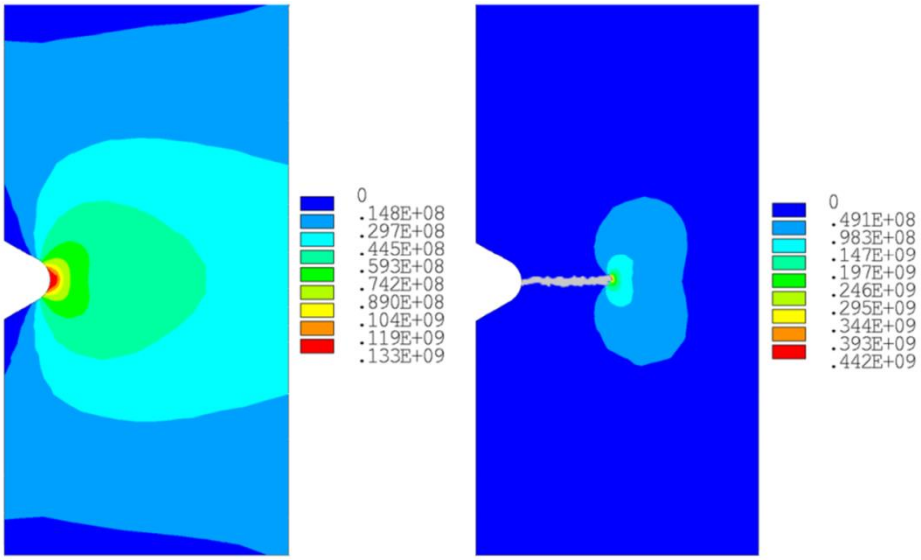


**Fig. 12.6.** V-notched Al-alloy specimen at $R$ = –1: **a** emergence of a "quasi-crack", **b** growth of a "quasi-crack".

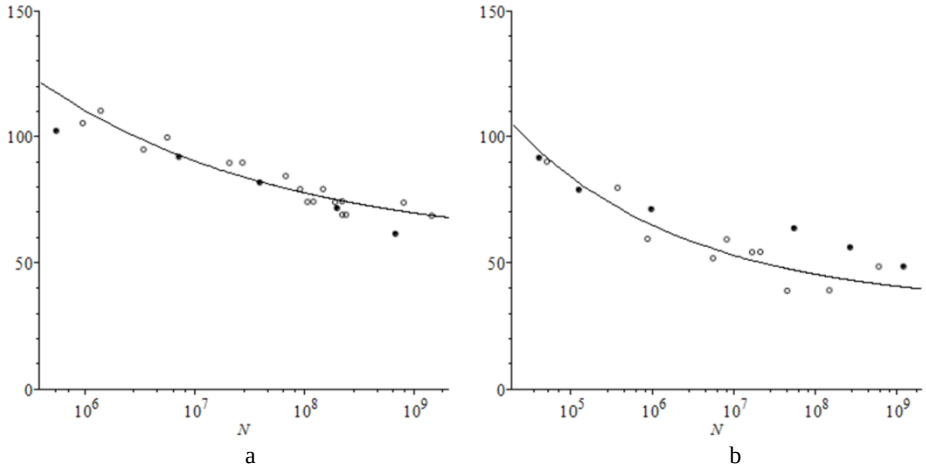


**Fig. 12.7.** VHCF fatigue curves $\sigma_{\max}(N)$ for V-notched Al-alloy specimen, where ○ means real test points, ● means calculating points: **a** $R$ = –1, **b** $R$ = 0.01.

Figures 12.6 and 12.7 show the calculation results for VHCF mode. In Fig. 12.7 the results of real and computational experiments on constructing fatigue curves for specimens with a side notch are presented. The curves in the figures approximate the experimental points for $R = -1$ (Fig. 12.7a) and $R = 0.01$ (Fig. 12.7b).

In Fig. 12.7, slight differences are observed between the calculated and experimental points. This can be explained as follows. The exponential exponent $\beta_{VH}$ of the fatigue curve for aluminium weakly depends on the cycle asymmetry coefficient $R$ [23, 37], but in the accepted calculating scheme with SWT criterion, this exponent is considered constant. Fig. 12.6 shows the lines of the effective stress level $\sigma_{VH}$ for the specimen with a notch in two states: before the fatigue quasi-crack initiation and at the moment when it has passed approximately halfway to macro-destruction.

## 12.5 Conclusions

A multi-mode kinetic model of cyclic loading damage development is proposed to describe the fatigue fracture process development. To determine the coefficients of the kinetic equation of damage, the well-known criterion of multiaxial fatigue failure SWT based on the mechanism associated with the development of microcracks of normal detachment is used.

A procedure has been proposed for calculating the kinetic equation coefficients for various fatigue failure modes of the LCF-HCF and VHCF. A numerical method for calculating crack-like zones up to macrofracture is proposed. The model parameters are determined from the condition of matching the experimental and calculated fatigue curve for a specimen of a certain geometry at a given load amplitude and cycle asymmetry coefficient. Using the obtained values, the results of experiments on specimens of a different geometry and asymmetry coefficients were reproduced and the model and calculation algorithm performance was confirmed.

### Acknowledgments

The study was carried out with a grant from the Russian Science Foundation (project No. 19-19-00705).

### References

1. Basquin, O.H.: The exponential law of endurance tests. Proc of the American society for testing and material 10, 625–630 (1910).
2. Brown, M., Miller, K.J.: A theory for fatigue under multiaxial stress-strain conditions. Institute of Mech. Engineers 187, 745–756 (1973).
3. Fatemi, A., Socie, D.F.: A critical plane approach to multiaxial damage including out-of-phase loading. Fatigue and Fracture of Eng. Materials and Structures 11(3), 149–156 (1988).

4. Smith, R.N., Watson, P., Topper, T.H.: A stress-strain parameter for the fatigue of metals. J. of Materials 5(4), 767–778 (1970).
5. Sines G., Behaviour of metals under complex static and alternating stresses. In: Sines, G, Waisman, J.L. (eds) Metal fatigue. New York: McGraw-Hill, pp. 145–169 (1959).
6. Crossland, B.: Effect of large hydrostatic pressures on torsional fatigue strength of an alloy steel. Proc. Int. Conf. on Fatigue of Metals, pp. 138–149. London (1956).
7. Findley, W.: A theory for the effect of mean stress on fatigue of metals under combined torsion and axial load or bending. J. of Eng. for Indust., 301–306 (1959).
8. Morel, F.: A critical plane approach for life prediction of high cycle fatigue under multiaxial variable amplitude loading. Int. J. of Fatigue 22(2), 101–119 (2000).
9. Matake, T.: An explanation on fatigue limit under combined stress. Bull JSME 20, 257–263 (1977).
10. McDiarmid D.L.: A shear stress based critical-plane criterion of multiaxial fatigue failure for design and life prediction. Fatigue Fract. Eng. Mater.Struct 17, 1475–1484 (1999).
11. Papadopoulos, I.V.: Long life fatigue under multiaxial loading. International Journal of Fatigue 23, 839–849 (2001).
12. Carpinteri, A., Spagnoli, A., Vantadori, S.: Multiaxial assessment using a simplified critical plane based criterion. Int. J. of Fatigue 33, 969–976 (2011).
13. Susmel, L., Taylor, D.: A critical distance/plane method to estimate finite life of notched components under variable amplitude uniaxial/multiaxial fatigue loading. Int. J. of Fatigue 38, 7–24 (2012).
14. Suman, S., Kallmeyer, A., Smith, J.: Development of a multiaxial fatigue damage parameter and life prediction methodology for non-proportional loading. Frattura ed Integrità Strutturale 38, 224–230 (2016).
15. Meggiolaro, M.A., Miranda, A.C., de Castro, J.: Comparison among fatigue life prediction methods and stress-strain models under multiaxial loading. Proceedings of 19th Int. Congress of Mech. Eng. Brasilia, DF, pp. 1–10 (2007).
16. Wang, Y.-Y., Yao, W.-X.: Evaluation and comparison of several multiaxial fatigue criteria. Int. J. of Fatigue 26, 17–25 (2004).
17. Karolczuk, A., Macha, E.: A review of critical plane orientations in multiaxial fatigue failure criteria of metallic materials. Int. J. of fatigue 134, 267–304 (2016).
18. Karolczuk, A., Papuga, J., Palin-Luc, T.: Progress in fatigue life calculation by implementing life-dependent material parameters in multiaxial fatigue criteria. Int. J. of Fatigue 134 (2020).
19. Bourago, N.G., Zhuravlev, A.B., Nikitin, I.S.: Models of multiaxial fatigue fracture and service life estimation of structural elements. Mechanics of Solids 46(6), 828–838 (2011).
20. Paris, P.C., Erdogan, F. A.: Critical analysis of crack propagation laws. J. Basic Engineering 85, 528–533 (1963).
21. Forman, R.G., Kearney, V.E., Engle, R.M.: Numerical analysis of crack propagation in a cyclic-loaded structure. Transactions ASME J Basic Eng. 89(3), 459–464 (1967).
22. Collins, J.A.: Failure of Materials in Mechanical Design: Analysis, Prediction, Prevention. Wiley, NY (1993).
23. Bathias, C., Paris, C.P.: Gigacycle fatigue in mechanical practice. Dekker, NY (2004).
24. Kachanov, L.M.: On the time of destruction under creep conditions. Izv. AN SSSR OTN 8, 26–31 (in Russian) (1958).
25. Rabotnov, J.N.: On the mechanism of long-term destruction. Voprosi prochnosti materialov i konstrukcij. AN SSSR OTN, 5–7 (in Russian) (1959).
26. Murakami, S.: Continuum Damage Mechanics. A Continuum Mechanics Approach to the Analysis of Damage and Fracture. Springer, Dordrecht (2012).

27. Altenbach H., Skrzypek J.J. (eds): Creep and Damage in Materials and Structures. Springer Vienna, Vienna (1999).
28. Lemaitre, J., Chaboche, J.L.: Mechanics of solid materials. Cambridge University Press (1994).
29. Marmi, A.K., Habraken, A.M., Duchene, L.: Multiaxial fatigue damage modeling at macro scale of Ti6Al4V alloy. Int. J. of fatigue 31, 2031–2040 (2009).
30. Zhi, Y.H., Wagner, D., Bathias, C., Chaboche, J.L.: Cumulative fatigue damage in low cycle fatigue and gigacycle fatigue for low carbon–manganese steel. Int. J. Fatigue 33, 115–121 (2011).
31. Fincato, R., Tsutsumi, S.: Coupled damage-viscoplasticity model for metals under cyclic loading conditions. Procedia Structural Integrity 18, 75–85 (2019).
32. Chaboche, J.L.: Time-independent constitutive theories for cyclic plasticity. International Journal of Plasticity 2(2), 149–188 (1986).
33. Burago, N.G., Nikitin, I.S.: Multiaxial Fatigue Criteria and Durability of Titanium Compressor Disks in low- and giga- Cycle Fatigue Modes. Mathematical Modeling and Optimization of Complex Structures, pp. 117-130. Springer, Heidelberg (2016).
34. Shanyavskiy, A.A., Soldatenkov, A.P.: The fatigue limit of metals as a characteristic of the multimodal fatigue life distribution for structural materials. Procedia Structural Integrity 23, 63–68 (2019).
35. Gates, N., Fatemi, A.: Multiaxial variable amplitude fatigue life analysis including notch effects. Int. J. of fatigue 91, 337–351 (2016).
36. Burago, N.G., Nikitin, I.S., Nikitin, A.D., Stratula, B.A.: Algorithms for calculation damage processes. Frattura ed Integrità Strutturale 49, 212–224 (2019).
37. Perez-Mora, R.: Study of the fatigue strength in the gigacycle regime of metallic alloys used in the aeronautics and off-shore industries. Thèse de doctorat en Mécanique. https://www.theses.fr/2010ENAM0027# (2010).